

A Physics-Informed Neural Network for the Calibration of Electromagnetic Navigation Systems

Pascal Ernst¹, Simone Gervasoni^{1,2}, Derick Sivakumaran^{1,2}, Enea Masina¹,
David Sargent^{1,2}, Bradley J. Nelson², Quentin Boehler²

Abstract—Electromagnetic Navigation Systems enable remote actuation of untethered micro and nanorobots, as well as the precise control of magnetic surgical tools for minimally invasive medical procedures. Accurate modeling of the magnetic fields generated by the electromagnets composing these systems is essential for achieving reliable and precise navigation. Existing modeling approaches either neglect nonlinear effects such as electromagnet saturation or fail to ensure that the field predictions are physically consistent. These limitations can lead to significant prediction errors, particularly in the estimation of field gradients, which directly impacts force calculations. As a result, inaccurate gradient predictions degrade force control performance, limiting the precision of magnetic actuation. In this work, we investigate physics-informed and data-driven modeling techniques to improve the accuracy of magnetic field and gradient predictions. Additionally, we introduce an approach for solving the inverse problem, developing models capable of predicting the required electromagnet currents to generate a desired magnetic field and gradient based on this approach. By incorporating physical constraints into the models, we enhance the predictive accuracy and physical consistency of the field estimates. In the experimental section, we demonstrate the benefits of these methods to enable improved force control in open-loop for untethered robots using a small-scale Electromagnetic Navigation System.

I. INTRODUCTION

From advanced robotics to biomedical applications, magnetic manipulation has emerged as a pivotal technology for non-invasive and precise control over objects of varying scales [1]. This technology uses a Magnetic Navigation System (MNS) to remotely actuate magnetized objects, with applications ranging from drug delivery and cellular manipulation to minimally invasive surgeries [2]. This approach has been used to investigate cellular behavior at the nanoscale [3], navigate micro- and millimeter-sized devices through complex environments using oscillating or rotating magnetic fields [4]–[7], and control larger devices for therapeutic and diagnostic applications [8]–[11]. An Electromagnetic Navigation System (eMNS) is a type of MNS composed of current-controlled electromagnets that is particularly suitable for generating dynamically changing magnetic fields [12].

Accurate modeling of magnetic fields generated by an eMNS is crucial to achieving precise control in medical and microrobotic systems [13]. Conventional methods, including Multipole Electromagnet Model (MPEM), utilize

This work was supported by the Swiss National Science Foundation through grant number 200020B_212885, and the ITC-InnoHK grant 16312.

¹ Magnebotix AG, Zurich, Switzerland pernst@ethz.ch

² Multi-Scale Robotics Lab, ETH Zurich, Switzerland qboehler@ethz.ch

linear approximations or numerical simulations, which do not account for nonlinear effects such as electromagnetic saturation, leading to substantial prediction errors at high field strengths [14], [15]. Data-driven techniques, such as Artificial Neural Network (ANN) and Convolutional Neural Network (CNN), have demonstrated improved accuracy by learning complex nonlinear relationships between currents and magnetic fields [15], [16]. However, they lack physical consistency, resulting in the violation of Maxwell's equations. Most existing methods are designed to predict the magnetic field from a given set of currents, while limited attention has been given to the inverse problem of calculating the necessary currents required to achieve a desired magnetic field and its spatial gradients.

This work introduces a modeling framework that integrates a Physics-Informed Neural Network (PINN) for the prediction of the magnetic fields and gradients generated by an eMNS. This framework promotes compliance with Maxwell's equations and enhances the physical consistency of the prediction. Models are also introduced to address the inverse problem. These models are designed to align with the predictions of the trained PINN, ensuring consistent and reliable performance. Experimental results demonstrate the effectiveness of the proposed approach, particularly in accurate gradient prediction and open-loop control scenarios.

The remainder of this paper is organized as follows. Section II provides an overview of the background and related work on the modeling of magnetic fields and eMNS. Section III introduces the proposed models based on PINN. In Section IV, the performance of the proposed models is evaluated and compared to existing methods. This section also includes open-loop control experiments of a permanent magnet to demonstrate the superiority of the PINN-based models. Conclusions are finally provided in Section V.

II. BACKGROUND AND RELATED WORKS

A. Forward and Backward Models

The mathematical model of an eMNS describes the relationship between the electrical currents passing through the electromagnets and the resulting magnetic field generated within the workspace at a specific position. The *forward model* predicts the magnetic field \mathbf{B} and its gradient $\nabla\mathbf{B}$ at a given position for specified currents through the electromagnets. This predictive capability is essential for determining the magnetic environment at any point within the workspace.

Conversely, the *backward model* determines the set of currents required to produce a desired magnetic field at a

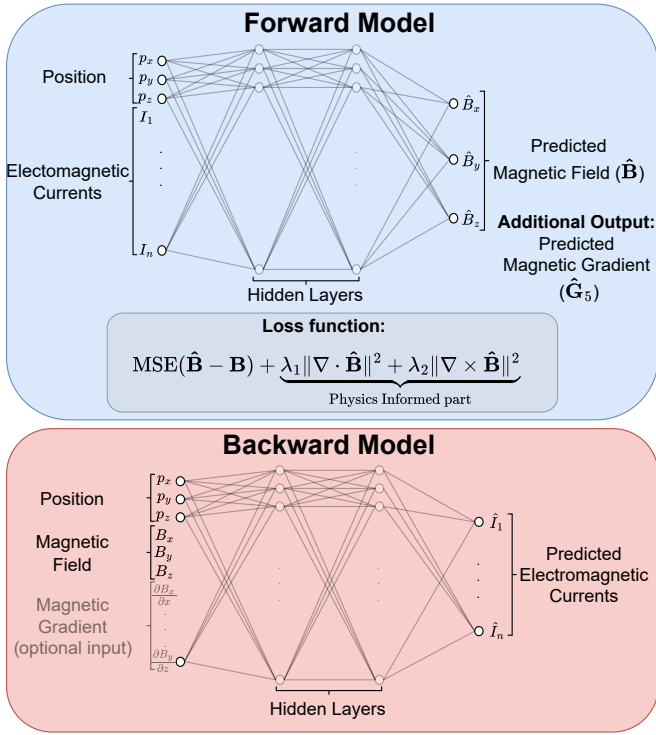


Fig. 1: Physics-informed neural networks models for electromagnetic navigation systems. The forward model takes the currents and position as inputs to predict the magnetic field and its gradient. The backward model computes the currents to generate a desired magnetic field and gradient.

given position. This model can be optimized by incorporating additional constraints to achieve specific objectives while ensuring the generation of the target magnetic field. One possible optimization criterion is the minimization of power consumption, which can be achieved by reducing the ℓ_2 -norm of applied currents. Furthermore, the backward model can be extended to incorporate the magnetic field gradient, enabling the computation of currents necessary to achieve both a specified magnetic field and gradient at a certain position. The backward model is essential for performing magnetic manipulation tasks. An overview of both models is given in Figure 1.

B. Modeling Magnetic Fields

The magnetic field generated at a given position in the workspace is represented by

$$\mathbf{B} = [B_x \ B_y \ B_z]^T \quad (1)$$

and adheres to Maxwell's equations:

$$\nabla \cdot \mathbf{B} = 0, \quad (2)$$

$$\nabla \times \mathbf{B} = 0. \quad (3)$$

Using these properties, the magnetic gradient represented by the 3×3 gradient matrix $\nabla \mathbf{B}$,

$$\nabla \mathbf{B} = \left[\frac{\partial \mathbf{B}}{\partial x} \quad \frac{\partial \mathbf{B}}{\partial y} \quad \frac{\partial \mathbf{B}}{\partial z} \right]^T, \quad (4)$$

can be further simplified. Since the gradient has only five independent parameters, the matrix in Equation (4) can be replaced by the reduced vector:

$$\mathbf{G}_5 = \left[\frac{\partial B_x}{\partial x} \quad \frac{\partial B_x}{\partial y} \quad \frac{\partial B_x}{\partial z} \quad \frac{\partial B_y}{\partial y} \quad \frac{\partial B_y}{\partial z} \right]^T. \quad (5)$$

Analytical models, such as MPEM, inherently guarantee divergence-free and curl-free fields due to their basis in Maxwell's equations [14]. However, these models are unable to capture non-linear effects such as electromagnetic saturation, leading to significant inaccuracies at high field strengths. In contrast, data-driven methods, including ANN and CNN, effectively learn complex nonlinear relationships between currents and magnetic fields [15], [16] but lack physical constraints resulting in predicted fields that violate Maxwell's equations. Although these violations might have minimal impact on the predicted magnetic field itself, they can cause substantial errors in the predicted field gradients. Such inaccuracies are particularly problematic in applications that require accurate force predictions, where gradient estimation is critical.

C. Interpolation of Magnetic Field Data

Magnetic field data, whether obtained from simulations or physical measurements, can be interpolated to construct a continuous field representation. Common techniques include trilinear, tricubic, and B-spline interpolation [15]. Interpolation relies only on the available magnetic field data, regardless of the specific eMNS model. As long as the measurements are accurate and have sufficient resolution, interpolation can provide a precise and continuous representation of the field without requiring complex model parameterization. However, for eMNS with multiple electromagnets, the dimensionality increases, making interpolation impractical when nonlinear magnetization effects prevent individual field contributions from being separated.

D. Multipole Electromagnet Model

The MPEM provides a linear model of an eMNS using a spherical multipole expansion to describe the magnetic scalar potential [14]. This ensures that the resulting field is curl-free and divergence-free, since it satisfies Laplace's equation. The model assumes a linear relationship between the magnetic field and the applied currents, enabling superposition to compute the total field. In practical applications, a low-order representation is often sufficient, as higher-order terms contribute negligibly; this simplification has been used in [17]–[20], where sources are modeled as dipoles. Although computationally efficient and physically consistent, it does not account for nonlinear effects introduced by ferromagnetic cores in the saturation region. The unknown coefficients, source positions, and orientations are typically determined through nonlinear least-squares optimization [21].

E. Machine Learning Models

Machine learning techniques have been applied to the forward model of an eMNS, as described in [16]. The modeling problem was formulated as a regression task, where the

inputs consisted of the electromagnet currents and the spatial position, while the output was the corresponding magnetic field vector. To address this problem, models including a Random Forest (RF) and an ANN were implemented. In [15], Charreyron et al. introduced methods based on CNN, which predict a discrete map of the magnetic field. This approach extends traditional regression models by using spatial patterns in the data. They also introduced a divergence-free model by predicting the magnetic vector potential instead of the magnetic field as the output of the network. Additionally, an unconstrained nonlinear solver was used to determine a set of currents that achieve a desired magnetic field while minimizing power consumption. This solver employs a regularized minimization approach, ensuring efficient current configurations while meeting the magnetic field requirements [15]. The dataset for both studies was generated using the CardioMag, a clinical-size eMNS equipped with eight large electromagnets. This system features a large workspace and exhibits nonlinear magnetization, with strong saturation occurring over 70% of its magnetic field generation capacity. Machine learning methods demonstrated significant improvements in magnetic field prediction accuracy compared to baseline MPEM. However, the CNN-based methods do not allow to derive an analytical representation of the positional derivatives of the field, limiting their applicability in scenarios requiring gradient information. Unlike these previous methods, the present work introduces a forward model which loss function penalizes the curl and divergence of the magnetic field. This minimizes the violation of the Maxwell equations, whereas the magnetic field and its gradient are directly predicted at the output of the network.

III. METHOD

A. Forward Model

We propose a forward model using a PINN to predict the magnetic field \mathbf{B} and its gradient \mathbf{G}_5 for a given set of input currents and positional coordinates. This approach integrates physical principles into the learning process to improve predictive accuracy and compliance with (2) and (3). In this work, the proposed models are evaluated on the MFG-100 (Magnebotix AG), a small-scale eMNS illustrated in Figure 2 comprising 8 electromagnets. The PINN architecture consists of an input layer with 11 neurons, corresponding to 3 positional arguments and 8 currents. These inputs are normalized so that all values lie between -1 and 1 . The loss function is defined as the weighted sum of three terms (see Figure 1):

- 1) The Mean Squared Error (MSE) between the predicted and measured magnetic field values.

- 2) The ℓ_2 -norm of the divergence of the predicted fields, promoting $\nabla \cdot \mathbf{B} = 0$.
- 3) The ℓ_2 -norm of the curl of the predicted fields, promoting $\nabla \times \mathbf{B} = 0$.

The gradients of the magnetic field are computed analytically using automatic differentiation. Early stopping is applied if the validation loss does not decrease over 10 consecutive epochs to prevent overfitting. The architecture and training setup are summarized in Table I, where CV denotes cross-validation, Opt. stands for optimizer, LR refers to the learning rate, and Act. stands for activation function.

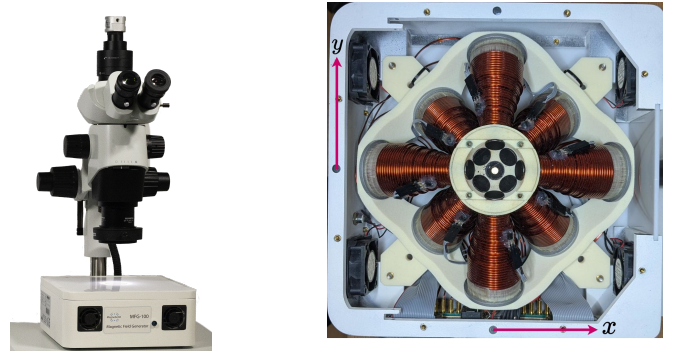


Fig. 2: The MFG-100 (Magnebotix AG), a compact eight-electromagnet eMNS. Left: system integrated with a microscope setup; Right: top-down view of the opened MFG-100.

B. Backward Models

The backward model is used to determine the necessary currents in the electromagnets to generate a desired magnetic field, and possibly its gradient, at a given position in space. For both backward models, the inputs are normalized to the range $[-1, 1]$, and the final layer uses a \tanh activation function with its output scaled by the maximum allowed current I_{max} , ensuring that the predictions are within $[-I_{max}, I_{max}]$. The early stopping is applied identically to the procedure described for the forward model, while the architecture and hyperparameter used are shown in Table I. Both backward models rely on a pre-trained and fixed forward model during training, making them sensitive to any inaccuracies or modeling errors in the forward model.

1) *Backward Model without Gradients:* This model is used to solve the inverse problem without specifying a desired gradient. The set of currents required to generate a magnetic field \mathbf{B} at a given position is predicted while minimizing the ℓ_2 -norm of the currents to ensure efficiency. This first approach is suitable for applications where high field magnitudes are prioritized over precise gradient control.

TABLE I: Used network architecture and hyperparameters.

Model	Hidden Layers	Opt.	Act.	LR	Batch Size	CV Folds	Epochs
Forward Model	[50, 100, 100]						
Backward Model (w/o \mathbf{G}_5)	[50, 100, 100]	Adam	\tanh	0.003	120	5	100
Backward Model (w/ \mathbf{G}_5)	[100, 200, 200]						

Supervised learning is not suitable for this model because the objective is not just to predict the required currents but also to minimize their ℓ_2 -norm. Since multiple current combinations can produce the same magnetic field at a given point, a supervised approach cannot ensure the selection of the optimal current set.

During training, this backward model receives a target position and a magnetic field vector as input and outputs a current prediction. This current is then passed through a fixed, pre-trained forward model to compute the resulting magnetic field. The loss is defined as the MSE between the predicted and target magnetic fields, augmented by a regularization term on the ℓ_2 -norm of the predicted currents:

$$\mathcal{L} = \|\mathbf{B}_{\text{target}} - \mathbf{B}_{\text{pred}}\|^2 + w\|\mathbf{I}_{\text{pred}}\|^2.$$

This approach enables the model to learn current configurations that generate the desired magnetic field while minimizing energy consumption. In practice, no instability or divergence was observed during training, and convergence was consistently achieved in all experiments. The regularization weight w was set to 0.01, and it was found to be highly sensitive, requiring careful tuning to achieve a good trade-off between accurate field reproduction and low current magnitude.

2) Backward Model with Gradients: The backward model predicts the set of currents required to generate a specified magnetic field \mathbf{B} and its spatial gradients, represented by \mathbf{G}_5 , at a given position. The inclusion of the gradient information allows for precise control over both the magnetic field and the forces acting on magnetic agents, making it suitable for applications requiring fine spatial control.

The model architecture accepts positional coordinates, magnetic field components, and the reduced gradient vector \mathbf{G}_5 as inputs. It is trained using a supervised learning approach on a dataset generated by a pre-trained forward model, which provides both field and gradient information. The loss function includes the MSE between predicted and target current values, which promotes accurate current estimation. This setup ensures consistency between the forward and backward models.

C. Hyperparameter Selection

A hyperparameter search was performed for all models in terms of batch size, learning rate, and number of training epochs using a random search approach. In contrast, other parameters, such as the weights in the loss terms (λ_1 , λ_2 and w) were empirically determined by iterative tuning. The network architecture for the forward model was adopted from

previous work [15], [16], which demonstrated strong performance in related tasks. The architectures for the backward models were then slightly modified to accommodate their distinct input-output structure.

D. Data Collection

The forward model of the MFG-100 is trained using a combination of a calibration and a verification dataset. The workspace is a cubic region with a side length of 2 cm. Calibration data are collected from a $10 \times 10 \times 10$ grid of measurement points, evenly distributed throughout the cubic region. At each grid point, uniformly random current vectors ranging from -18 A to 18 A are applied, producing a dataset of 50,000 data points. The magnetic field is measured using a three-axis Hall magnetometer (THM1176, Metrolab) that was positioned across the workspace using a FUYU Gantry Robot XYZ Stage.

The verification dataset consists of random points within the workspace. At these points, random current vectors are again applied, and the magnetic field is measured using the same magnetometer. The verification dataset consists of 1330 distinct data points.

E. Evaluation Methods

The following performance metrics are evaluated to quantify the accuracy of the prediction and the physical consistency of the models.

The Root Mean Squared Error (RMSE) measures the average magnitude of the error between the predicted and target values:

$$\text{RMSE} = \sqrt{\frac{1}{N} \sum_{i=1}^N \|\mathbf{y}_i - \hat{\mathbf{y}}_i\|^2}, \quad (6)$$

where \mathbf{y}_i represents the target values, $\hat{\mathbf{y}}_i$ represents the predicted values and N is the total number of data points.

The coefficient of determination (R^2) is calculated to evaluate how well the model predictions align with the observed data:

$$R^2 = 1 - \frac{\sum_{i=1}^N \|\mathbf{y}_i - \hat{\mathbf{y}}_i\|^2}{\sum_{i=1}^N \|\mathbf{y}_i - \bar{\mathbf{y}}\|^2}, \quad (7)$$

where $\bar{\mathbf{y}}$ is the mean of the target values. An R^2 value closer to 1 signifies a higher degree of predictive accuracy.

To assess if the predicted magnetic fields adhere to Maxwell's equations, the mean curl norm and the mean divergence norm are computed as well. The mean curl norm

TABLE II: Comparison of physics-weighted forward-model performances.

Physics Weights		RMSE (mT)	R^2	Mean Curl Norm (T/m)	Mean Div. Norm (T/m)	Time/Step (s)
Divergence (λ_1)	Curl (λ_2)	1.88	0.993	20.9 ± 3.37	33.9 ± 20.09	2.89
0.0	0.0	5.98	0.938	26.0 ± 8.16	8.2 ± 1.35	3.70
0.15	0.0	4.88	0.958	10.7 ± 2.19	20.2 ± 4.75	4.15
0.0	0.15	3.24	0.981	12.5 ± 1.52	6.1 ± 1.57	3.61
0.15	0.15	3.81	0.974	8.0 ± 0.81	3.0 ± 0.46	3.58
0.3	0.3	3.81	0.974	6.5 ± 0.95	3.3 ± 1.00	3.64
0.5	0.5	7.29	0.907			

measures the average deviation of the magnetic field from being curl-free:

$$\text{Mean Curl Norm} = \frac{1}{N} \sum_{i=1}^N \|\nabla \times \mathbf{B}_i\|, \quad (8)$$

where \mathbf{B}_i is the predicted magnetic field at the i th data point. The mean divergence norm measures the deviation from being divergence-free:

$$\text{Mean Divergence Norm} = \frac{1}{N} \sum_{i=1}^N \|\nabla \cdot \mathbf{B}_i\|. \quad (9)$$

These metrics collectively provide a comprehensive evaluation of the models, capturing both prediction accuracy and adherence to physical principles, with lower values for the curl and divergence norms indicating better compliance with Maxwell's equations.

IV. RESULTS

A. Forward Model

Table II presents a comparison of the performance of the forward model under varying physics-based regularization weights λ_1 and λ_2 . The model with $\lambda_1 = \lambda_2 = 0.0$ corresponds to the purely data-driven baseline ANN, while the configuration with $\lambda_1 = \lambda_2 = 0.15$ defines the proposed PINN.

The ANN achieves the lowest RMSE and the highest R^2 value, indicating the strongest predictive accuracy for the magnetic field. However, it exhibits the largest violation of Maxwell's constraints. Increasing the physics weights improves physical consistency at the cost of prediction accuracy. The PINN strikes a balance by significantly reducing both divergence and curl, while maintaining a good RMSE and R^2 value. Further increasing the weights reduces divergence and curl even more, but leads to degraded predictive performance. This highlights a trade-off between data fidelity and physical consistency, controlled by the regularization weights.

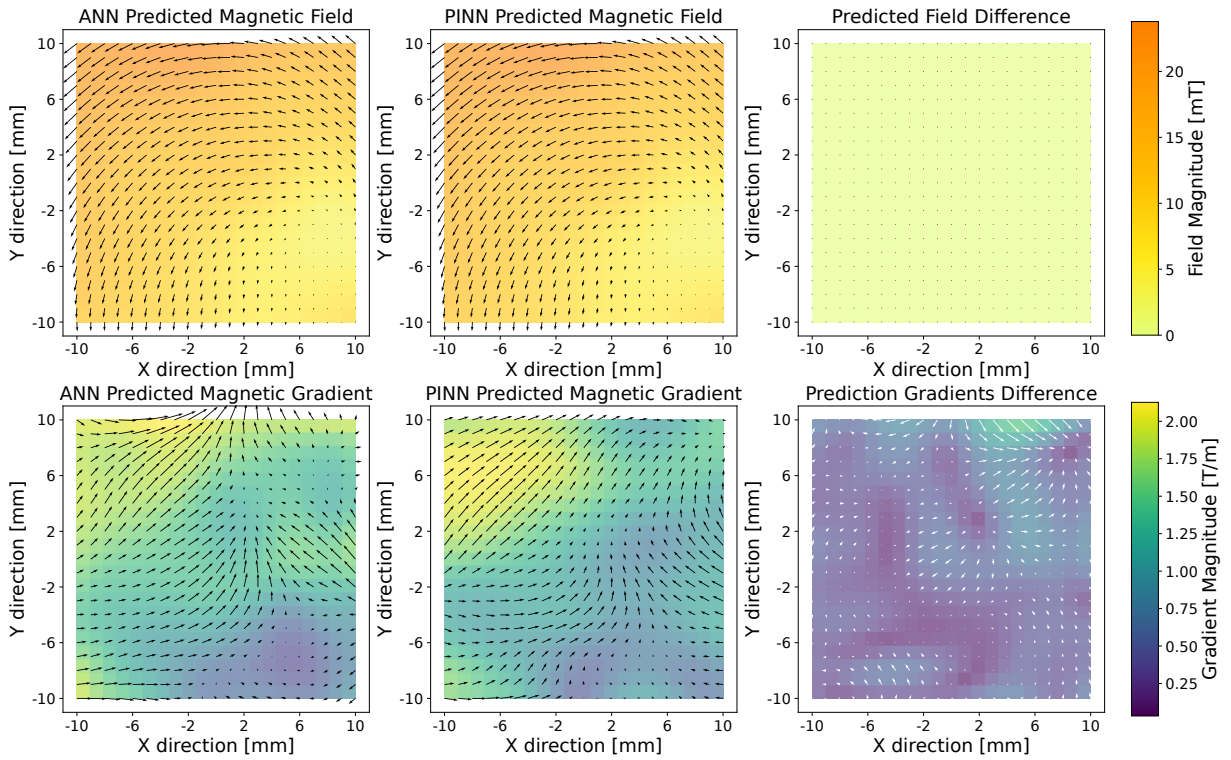


Fig. 3: Comparison of magnetic field and gradient predictions for ANN and PINN models of the MFG-100. The left column shows the magnetic field (top) and magnetic gradient (bottom) predicted by the ANN. The middle column presents the corresponding predictions from the PINN. The right column visualizes the discrepancies between the two models, highlighting the discrepancies in both field and gradient predictions. In the gradient plots, the arrows represent the direction of the force acting on a dipole with a magnetic dipole moment magnitude of 1 aligned with the magnetic field direction. The magnitude shown corresponds to the force experienced by the dipole.

All models were evaluated on the same system (12th Gen Intel® Core™ i7 CPU). The calibration speed of the PINN is slightly lower than that of the ANN, but since this calibration is performed only once per system prior to experimentation, the increased runtime is not critical.

B. Field and Gradient Predictions

To further illustrate the predictive performance of the models, Figure 3 presents a comparison of the predicted magnetic field and gradient distributions for a specific set of input currents. The ANN and PINN predictions are shown separately, along with the differences in their respective field and gradient predictions. Although both ANN and PINN provide similar magnetic field predictions, the differences in the gradient predictions are significant. This indicates that despite the field predictions appearing accurate, the spatial variations captured by each model differ considerably. Accurate gradient predictions are crucial for force and torque calculations, as demonstrated in the open-loop experiment presented in Section IV-D, where the PINN model contributes to more precise trajectory tracking.

C. Backward Model

1) Backward Model without Gradients: The backward model without gradients achieves an RMSE of 0.7 mT and an R^2 value of 0.999, indicating highly accurate current predictions for generating the desired magnetic fields. Those results are obtained using a trained PINN model. Similar results are obtained using a trained ANN.

2) Backward Model with Gradients: The backward model with gradients, when trained on data generated by a trained PINN, achieves an R^2 value of 0.936 and an RMSE of 0.567 A. In contrast, the same model trained on data generated by a trained ANN achieves a lower R^2 value of 0.884 and a higher RMSE of 0.785 A.

D. Open-Loop Control of a Permanent Magnet

An experiment was conducted to evaluate the control of a permanent magnet in open loop, which constitutes a benchmark experiment for assessing the quality of the model. A magnetic cube with a side length of 1 mm was placed within the workspace of the MFG-100 and subjected to a controlled magnetic force \mathbf{F} governed by

$$\mathbf{F} = (\mathbf{m} \cdot \nabla) \mathbf{B}. \quad (10)$$

The magnetic dipole moment \mathbf{m} of the cube was assumed to be aligned with the applied magnetic field \mathbf{B} . The field was configured to match the desired force direction, enabling controlled propulsion through spatial gradients of the magnetic field.

The applied force was constrained to the x-y plane (see Figure 2) and computed based on the required position trajectory, accounting for Coulomb friction effects. The opposing frictional force was modeled as:

$$\mathbf{F}_f = -\mu \mathbf{N} \frac{\mathbf{v}}{\|\mathbf{v}\|}, \quad (11)$$

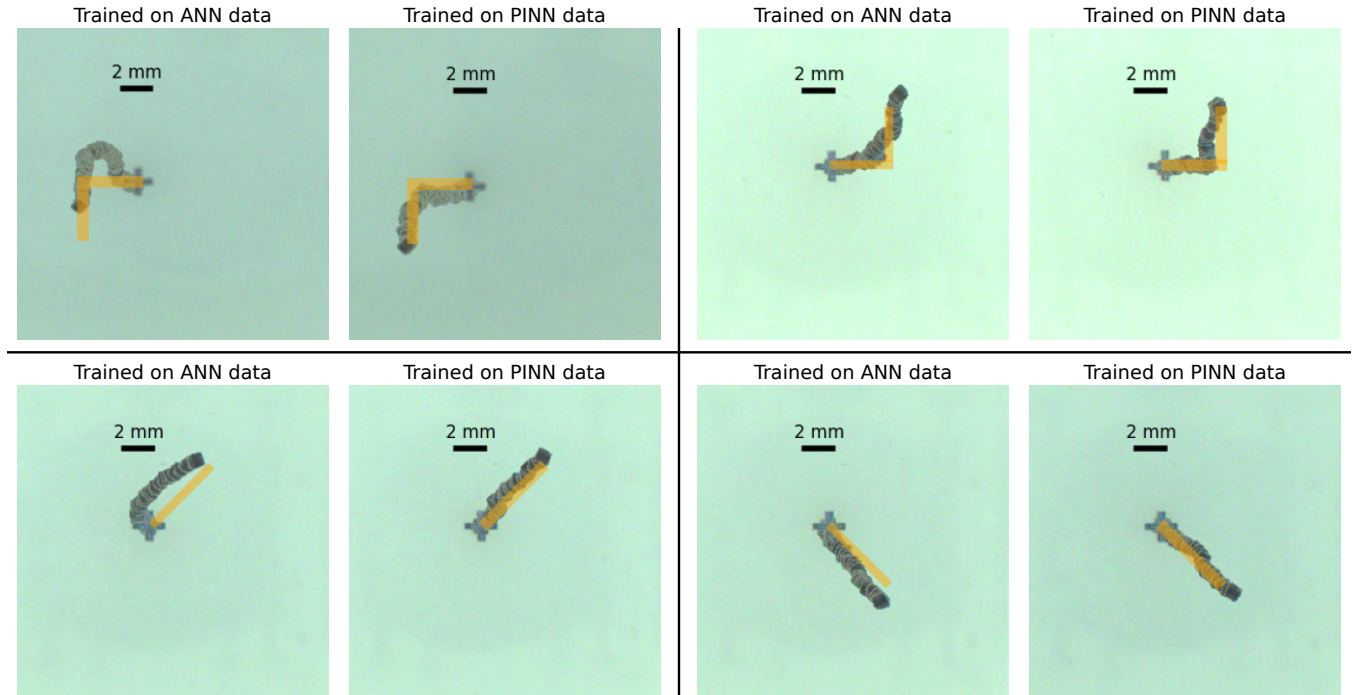


Fig. 4: Comparison of open-loop controlled magnet trajectories with the MFG-100 using backward models with gradients trained on ANN and PINN data. The top row presents the best trials for L-shaped trajectories, with the left plot showing movement to the left and the right plot showing movement to the right. The bottom row illustrates diagonal trajectories, where the left plot represents movement toward the top right, and the right plot represents movement downward and to the right.

where μ is the friction coefficient, \mathbf{N} is the normal force and \mathbf{v} is the velocity of the magnet.

The motion of the magnet was estimated using a kinematic model incorporating its mass m , the net applied force, and the frictional resistance:

$$m \frac{d\mathbf{v}}{dt} = \mathbf{F} + \mathbf{F}_f, \quad (12)$$

Since motion is restricted to the x-y plane, both the velocity vector \mathbf{v} and the position vector \mathbf{r} are two-dimensional. The position of the magnet was then updated using the following:

$$\mathbf{r}(t + \Delta t) = \mathbf{r}(t) + \mathbf{v}(t)\Delta t, \quad (13)$$

where \mathbf{r} is the position vector and Δt , which is set to 0.025 seconds, is the time step. This approach allows for accurate computation of the applied force and realistic simulation of the magnet's motion by considering the combined effects of the magnetic force, friction, and inertia. The observed currents were around 1 A.

The gradient $\nabla \mathbf{B}$ was calculated using Equation 10 and the required currents were determined at predefined positions along the trajectory using the trained backward models.

The experiment evaluated the performance of the backward model with gradients trained on data generated by the ANN and PINN models. Four different trajectories were tested. For each trajectory, three experimental trials were recorded to ensure repeatability. The best trial for each case is illustrated in Figure 4. Additionally, the maximal deviation of the magnet's center from the predefined trajectory was assessed.

The backward model trained on PINN data achieved a mean maximal deviation across all runs of 1.134 ± 0.623 mm, while the model trained on ANN data resulted in a higher deviation of 2.123 ± 0.640 mm.

V. CONCLUSION

Accurate modeling of the magnetic fields and gradients in eMNS is crucial for precise force control in microrobotic applications. This work introduces a PINN-based forward model to predict magnetic fields and gradients from a given set of currents, promoting compliance with Maxwell's equations and enhancing physical consistency. Although the ANN model without physical constraints achieved the highest field prediction accuracy, the PINN model demonstrated superior physical consistency by promoting compliance with Maxwell's equations through its loss function. This work also introduced the training of a neural network-based backward model capable of predicting the required currents to generate a desired magnetic field and its gradients, with the PINN-trained variant achieving higher accuracy than the ANN-trained counterpart. Open-loop control experiments validated these findings, showing that the PINN-trained model resulted in significantly lower trajectory deviations. The experimental results also highlight the importance of incorporating physics-informed constraints in learning-based models to improve field and gradient predictions, ultimately improving force-based control in electromagnetic actuation.

REFERENCES

- [1] L. Wang, Z. Meng, Y. Chen, and Y. Zheng, "Engineering magnetic micro/nanorobots for versatile biomedical applications," *Adv. Intell. Syst.*, vol. 3, no. 7, p. 2000267, 2021.
- [2] J. Li, B. Esteban-Fernández de Ávila, W. Gao, L. Zhang, and J. Wang, "Micro/nanorobots for biomedicine: Delivery, surgery, sensing, and detoxification," *Sci. Robot.*, vol. 2, no. 4, p. eaam6431, 2017.
- [3] S. Schuerle, S. Erni, M. Flink, B. E. Kratochvil, and B. J. Nelson, "Three-dimensional magnetic manipulation of micro-and nanostructures for applications in life sciences," *IEEE Trans. Magn.*, vol. 49, no. 1, pp. 321–330, 2012.
- [4] A. Servant, F. Qiu, M. Mazza, K. Kostarelos, and B. J. Nelson, "Controlled *in vivo* swimming of a swarm of bacteria-like microrobotic flagella," *Adv. Mater.*, vol. 27, no. 19, pp. 2981–2988, 2015.
- [5] L. Zhang, T. Petit, K. E. Peyer, and B. J. Nelson, "Targeted cargo delivery using a rotating nickel nanowire," *Nanomedicine: NBM*, vol. 8, no. 7, pp. 1074–1080, 2012.
- [6] E. Diller, J. Zhuang, G. Zhan Lum, M. R. Edwards, and M. Sitti, "Continuously distributed magnetization profile for millimeter-scale elastomeric undulatory swimming," *Appl. Phys. Lett.*, vol. 104, no. 17, 2014.
- [7] K. Ishiyama, M. Sendoh, A. Yamazaki, M. Inoue, and K. I. Arai, "Swimming of magnetic micro-machines under a very wide-range of reynolds number conditions," *IEEE Trans. Magn.*, vol. 37, no. 4, pp. 2868–2870, 2001.
- [8] S. Ernst, F. Ouyang, C. Linder, K. Herting, F. Stahl, J. Chun, H. Hachiya, D. Bansch, M. Antz, and K.-H. Kuck, "Initial experience with remote catheter ablation using a novel magnetic navigation system: magnetic remote catheter ablation," *Circulation*, vol. 109, no. 12, pp. 1472–1475, 2004.
- [9] P. R. Slawinski, A. Z. Tadese, K. B. Musto, K. L. Obstein, and P. Valdastri, "Autonomous retroflexion of a magnetic flexible endoscope," *IEEE Robot. Autom. Lett.*, vol. 2, no. 3, pp. 1352–1359, 2017.
- [10] H. Andrew *et al.*, "Novel, magnetically guided catheter for endocardial mapping and radiofrequency catheter ablation," *Circulation journal: official journal of the Japanese Circulation Society*, vol. 67, p. 37, 2003.
- [11] A. J. Petruska and J. J. Abbott, "Omnimagnet: An omnidirectional electromagnet for controlled dipole-field generation," *IEEE Trans. Magn.*, vol. 50, no. 7, pp. 1–10, 2014.
- [12] Z. Yang and L. Zhang, "Magnetic actuation systems for miniature robots: A review," *Adv. Intell. Syst.*, vol. 2, no. 9, p. 2000082, 2020.
- [13] J. J. Abbott, E. Diller, and A. J. Petruska, "Magnetic methods in robotics," *Annu. Rev. Control Robot.*, vol. 3, no. 1, pp. 57–90, 2020.
- [14] A. J. Petruska, J. Edelmann, and B. J. Nelson, "Model-based calibration for magnetic manipulation," *IEEE Trans. Magn.*, vol. 53, no. 7, pp. 1–6, 2017.
- [15] S. L. Charreyron, Q. Boehler, B. Kim, C. Weibel, C. Chautems, and B. J. Nelson, "Modeling electromagnetic navigation systems," *IEEE Trans. Robot.*, vol. 37, no. 4, pp. 1009–1021, 2021.
- [16] R. Yu, S. L. Charreyron, Q. Boehler, C. Weibel, C. Chautems, C. C. Poon, and B. J. Nelson, "Modeling electromagnetic navigation systems for medical applications using random forests and artificial neural networks," in *2020 IEEE In. Conf. Robot. Autom.* IEEE, 2020, pp. 9251–9256.
- [17] R. Dreyfus, Q. Boehler, and B. J. Nelson, "A simulation framework for magnetic continuum robots," *IEEE Robot. Autom. Lett.*, vol. 7, no. 3, pp. 8370–8376, 2022.
- [18] H. Gu, Q. Boehler, H. Cui, E. Secchi, G. Savorana, C. De Marco, S. Gervasoni, Q. Peyron, T.-Y. Huang, S. Pane *et al.*, "Magnetic cilia carpets with programmable metachronal waves," *Nat. Commun.*, vol. 11, no. 1, p. 2637, 2020.
- [19] S. L. Charreyron, Q. Boehler, A. N. Danun, A. Mesot, M. Becker, and B. J. Nelson, "A magnetically navigated microcannula for subretinal injections," *IEEE Trans. Biomed. Eng.*, vol. 68, no. 1, pp. 119–129, 2020.
- [20] S. Gervasoni, N. Pedrini, T. Rifai, C. Fischer, F. C. Landers, M. Mattmann, R. Dreyfus, S. Viviani, A. Veciana, E. Masina *et al.*, "A human-scale clinically-ready electromagnetic navigation system for magnetically-responsive biomaterials and medical devices," *Adv. Mater.*, p. 2310701, 2024.
- [21] D. W. Marquardt, "An algorithm for least-squares estimation of nonlinear parameters," *J. Soc. Ind. Appl. Math.*, vol. 11, no. 2, pp. 431–441, 1963.